

EXPERIMENTS PRODUCING NANOPATTERNED ELECTRON BEAMS*

L.E. Malin[†], W.S. Graves, J.C.H. Spence, K. Weiss, and C. Zhang, Arizona State University, Tempe, USA
 R.K. Li, E.A. Nanni, X. Shen, S.P. Weathersby, and J. Yang
 SLAC National Accelerator Laboratory, Menlo Park, USA

Abstract

RF photoinjectors are increasingly used to image at the nanoscale in much the same way as a Transmission Electron Microscope (TEM), which are generally sub-MeV energy. We have conducted electron diffraction experiments through a thin membrane of single crystal silicon using both the TEM and photoinjector, and have been able to model and predict the diffraction patterns using the multislice method. A nanopatterned single crystal silicon grating was also imaged in the TEM in the bright field, where all but the direct beam of the diffraction pattern is blocked, giving high contrast spatial modulations corresponding to the 400 nm pitch grating lithographically etched into the silicon. Drawing from our previous multislice calculations, we determined the crystallographic orientation that maximized the contrast in this spatial modulation at the energy of the TEM, giving a bunching factor comparable to a saturated FEL. We report on these key steps toward control of radiation phase and temporal coherence in an FEL.

INTRODUCTION

With the increasing quality of RF photoinjector beams, techniques that were exclusive to transmission electron microscopes (TEM) can now be performed at the higher energies associated with these guns, such as viewing the diffraction pattern of a material or forming the real space image. Extending the parallels further, by selecting particular diffraction spots, features of the sample can be highlighted, increasing contrast and illuminating the nanoscale. If one were to replace the sample with a nanopatterned spatial mask, imaging these features can create an electron beam with a similar nanopattern. In conjunction with an emittance exchange (EEX) beam line, these spatial masks can be used to design a temporal distribution, allowing for the creation of a prebunched beam that can in turn produce coherent hard X-rays with inverse Compton scattering [1, 2].

THEORETICAL BACKGROUND

To be able to image a sample with an RF photoinjector in much the same way a TEM does, the beam quality must be sufficiently high that the individual diffraction spots are discernible without any overlap. To quantify this condition, we start with the Bragg angle for a material with a cubic crystal lattice:

* Work supported by NSF awards 1632780 and 1231306, DOE award DE-AC02-76SF00515, and the SLAC UED/UEM Initiative Program Development Fund.

[†] lemalin@asu.edu

$$\theta_B = \sin^{-1} \left(\frac{\lambda}{2a_0} \sqrt{h^2 + k^2 + l^2} \right) \quad (1)$$

where λ is the deBroglie wavelength of the electron, a_0 is the lattice parameter, and h, k, l are the Miller indices of the Bragg reflection. As long as the angular spread of the beam is less than this value, then the boundaries of the reflections are visible and the higher order Bragg reflections can be blocked. In the case of our setup, the closest allowed Bragg spots for Silicon (100) are the {220} family of reflections. For 2.26 MeV electrons, this corresponds to a Bragg angle of 1.2 mrad. For a beam with a known emittance, we can use this angular limit to define the minimum spot size. We recall that the normalized emittance at a waist is

$$\epsilon_n = \beta \gamma \sigma_x \sigma_{x'} \quad (2)$$

where β is the normalized velocity, γ is the Lorentz factor, σ_x is the RMS-width of the beam, and $\sigma_{x'}$ is the RMS beam divergence. Assuming a Gaussian angular distribution, the Bragg spots will be easily discernible if $\sigma_{x'} \leq \frac{\theta_B}{2}$ though decreasing the angular spread below this will increase the contrast as the overlap is lessened. Combining Eq. (1) and Eq. (2) with these condition, yields the following condition on our spot size, limiting the minimum number of periods that may be included in a single pulse and thus the maximum bandwidth:

$$\sigma_x < \frac{2\epsilon_n}{\beta \gamma \sin^{-1} \left(\frac{\lambda}{2a_0} \sqrt{h^2 + k^2 + l^2} \right)} \quad (3)$$

The orientation of the diffracting material also affects the observed contrast and must be chosen to maximize the associated modulation. To quantify the quality of the this contrast, we use the spatial Fourier transform as given by the bunching factor:

$$b_0 = \frac{1}{N_e} \sum_{p=1}^{N_e} e^{2\pi i \frac{x_p}{\lambda_x}} \quad (4)$$

where N_e is the number of electrons, x_p is the transverse position of the p^{th} particle, and λ_x is the wavelength of the spatial modulation. When determining the quality, the absolute value of Eq. (4) is used, giving a value between $1/N_e$ (shot noise) and 1 (perfectly ordered) at each surveyed wavelength.

IMAGING RESULTS

In both experiments, our sample was a 200nm thick single crystal Si(100) membrane, though in the TEM a nanopattern

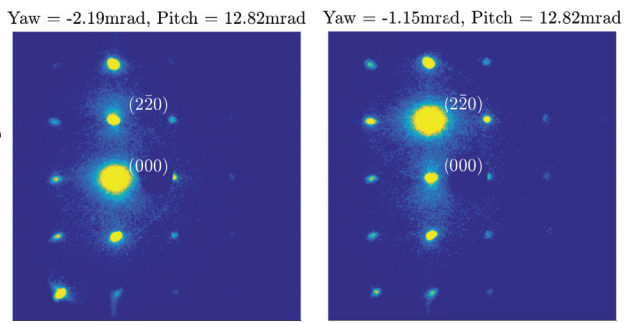


Figure 1: Diffraction patterns of 200 nm thick Si(100) membrane at two different crystallographic orientations relative to a 2.26 MeV electron beam (contrast enhanced and saturated).

was etched through the surface to create a grating. Currently, optics are being developed for the future photoinjector beamline at Arizona State University (ASU) to facilitate viewing both the diffraction plane and the image plane [3]. The pattern had a pitch of 400 nm, alternating between grooves of the original 200 nm thick silicon and cuts clear through the material.

RF Photoinjector

At the ASTA UED facility at SLAC [4], we previously used the multislice method to predict the intensity distribution of the diffraction pattern as the crystallographic orientation of the sample was varied [5, 6]. The diffraction pattern on the left side of Fig. 1 shows the orientation where approximately 80% of the elastically scattered beam finds its way into the direct beam (i.e. (000)). The image on the right shows the orientation where only about 5% of the elastically scattered beam is in the direct beam. Supposing we use a nanopatterned grating and given an aperture to block all but the direct beam and the requisite optics to view the image plane, what would result would be the bright field image matching the pattern produced not by absorption contrast, but by diffraction contrast. As for the inelastic background, in the bright field regime, and at the orientations at the top of Fig. 1, the majority can be blocked by making the aperture sufficiently small - the inelastic background is centered about the brightest spot in the pattern and decays with a Lorentzian distribution.

TEM

The etched grating was imaged in a FEI Titan ETEM at 300 keV (the upper two rows of Fig. 2) as well as Philips CM200-FEG TEM/STEM at 200 keV (the bottom row of Fig. 2) at the John M. Cowley Center for High Resolution Electron Microscopy at ASU. Due to the thickness of the membrane frame (500 μm), the grating would not fit in a conventional double-tilt holder, so we maximized the observed contrast in the profile along a single tilt axis. An aperture was then placed after the sample to block all but the direct beam (see Fig. 1), giving the bright field image.

In the current density plot, we can see up to an 8:1 contrast ratio between the valleys and the peaks, yielding a bunching factor of 0.414, which is comparable to the bunching factor of a saturated FEL. Based on previous multislice calculations at 300 keV, the intensity of the valleys (the portions of the grating with material) can be reduced to give a contrast ratio of 100:3, which will further increase the bunching factor. The lesser contrast on the upper two rows can be attributed to the mounting angle of the sample in the holder having changed between machines, causing the single-tilt axis to traverse a different set of angles. Furthermore, there are Fresnel fringes between the peaks in these images - an interference effect that reduces the sharpness of the edges and distorts the image.

Table 1: Bandwidth of Each Image

Number of Periods	FWHM (nm)
98	5.2
25	20.4
12	50.6

Fitting a Gaussian to the bunching factor plots in Fig. 2, we estimate the FWHM bandwidth values found in Table 1. A cursory look shows the pulses are approximately transform limited with the bandwidth decreasing as the number of periods in the pulse is increased. Furthermore, as more periods over a greater area are included, the wavelength of the peak bunching factor shifts closer to the 400 nm pitch value of the grating. This can be attributed to local variation in the etching being averaged as more of the pattern is included in the calculation as well as the Fresnel fringes distorting the peaks, especially in the images in the third row of Fig. 2.

CONCLUSION

Using bright field imaging in a TEM, a nanoscale modulation was produced that had a bunching factor comparable to a saturated FEL. With the development of samples that fit into standard two axis holders, this value is sure to increase. Furthermore, having shown that a RF photoinjector has the beam quality needed to image the diffraction pattern, we can infer that the introduction of an aperture to block all but the direct beam would result in a similar output to the TEM at the image plane of a future focusing system. By demagnifying this output and using an EEX, the resulting temporal modulation will serve as the the next step in converting the X-ray compact light source currently being commissioned by ASU into an XFEL.

ACKNOWLEDGEMENT

We gratefully acknowledge financial support from NSF awards 1632780 and 1231306, the BioXFEL Science and Technology Center, U.S. DOE Contract No. DE-AC02-76SF00515, and the SLAC UED/UEM Initiative Program

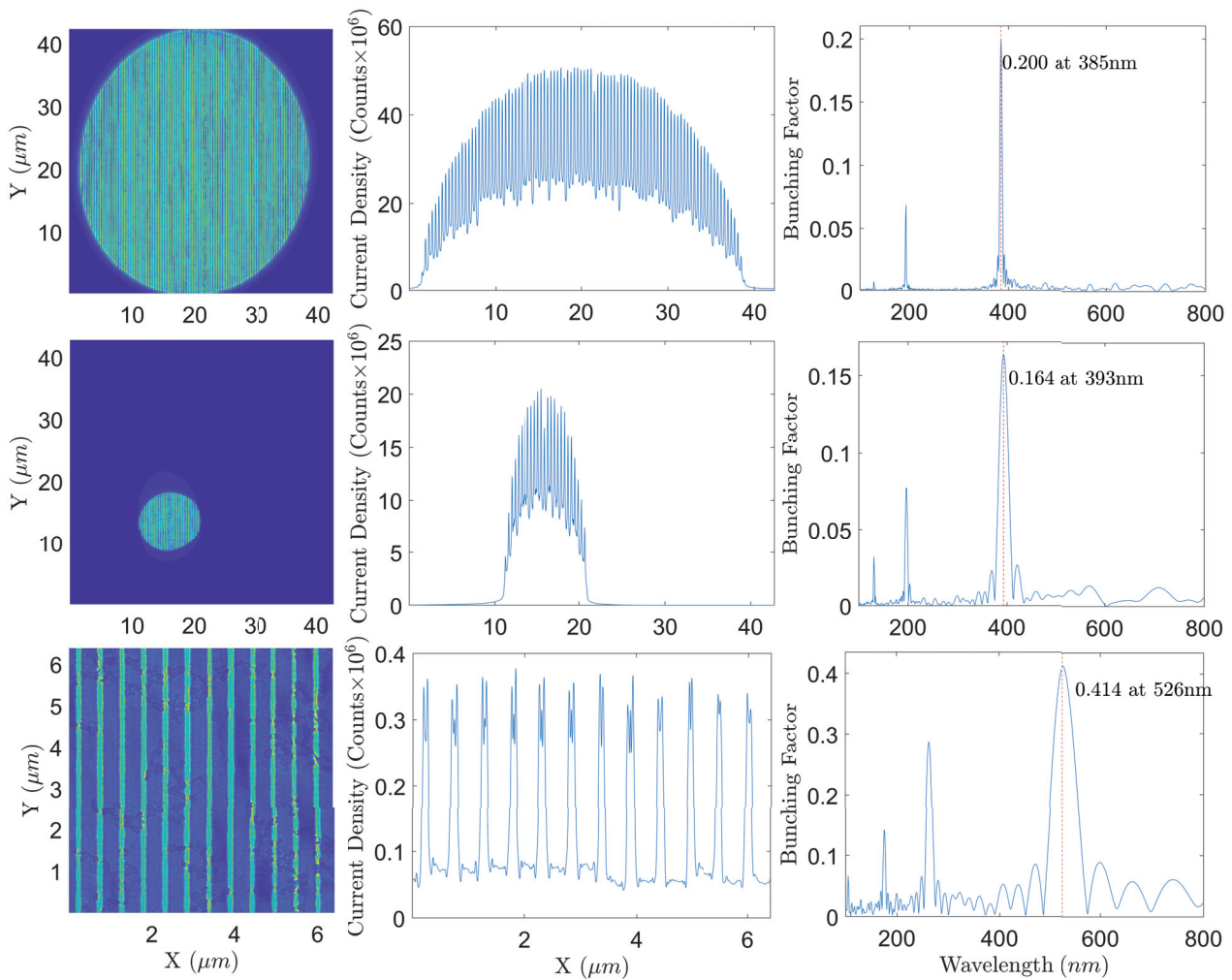


Figure 2: The TEM bright field image (left), current density in counts $\times 10^6$ (middle) and the calculated bunching factor $|b_0|$ are plotted for a $40 \mu\text{m}$ (upper row) spot size at $380\times$ magnification, $10 \mu\text{m}$ (middle row) spot size at $420\times$ magnification, and a close up of the membrane at $2550\times$ magnification. The first two rows have the same crystallographic orientation, while the third row does not, as the measurement was performed after having remounted the sample in a new holder.

Development Fund. We also acknowledge the use of facilities in the John M. Cowley Center for High Resolution Electron Microscopy at Arizona State University.

REFERENCES

- [1] W. S. Graves *et al.*, “ASU compact XFEL”, in *Proc. 38th International Free-Electron Laser Conference (FEL'17)*, Santa FE, USA, August 2017, paper TUB03.
- [2] E. A. Nanni, W. S. Graves, and D. E. Moncton, “Nanomodulated electron beams via electron diffraction and emittance exchange for coherent x-ray generation”, *Phys. Rev. Accel. Beams*, vol. 21, p. 014401, Jan 2018.
- [3] C. Zhang *et al.*, “Electron beam optics for the ASU compact XFEL”, in *Proc. 9th International Particle Accelerator Conference (IPAC'17)*, Vancouver, Canada, May 2018, paper TUPMK009.
- [4] S. P. Weathersby *et al.*, “Mega-electron-volt ultrafast electron diffraction at slac national accelerator laboratory”, *The Review of scientific instruments*, vol. 86, no. 7, p. 073702, 2015.
- [5] L. Malin *et al.*, “Comparison of theory, simulation, and experiment for dynamical extinction of relativistic electron beams diffracted through a si crystal membrane”, in *Proc. 8th International Particle Accelerator Conference (IPAC'17)*, Copenhagen, Denmark, May 2017, paper THPAB088, pp. 3924–3927.
- [6] C. Zhang *et al.*, “Experiments in electron beam nanopatterning”, in *Proc. 38th International Free-Electron Laser Conference (FEL'17)*, Santa FE, USA, August 2017, paper TUP038.